IEEE Access
Multidisciplinary | Rapid Review | Open Access Journal

Received February 11, 2019, accepted February 21, 2019, date of publication March 11, 2019, date of current version April 2, 2019.

Digital Object Identifier 10.1109/ACCESS.2019.2904249

Wideband, Beam-Steerable Reflectarrays Based on Minimum-Switch Topology, Polarization-Rotating Unit Cells

HUNG LUYEN, (Member, IEEE), ZONGTANG ZHANG, (Student Member, IEEE), JOHN H. BOOSKE, (Fellow, IEEE), AND NADER BEHDAD, (Fellow, IEEE)
Department of Electrical and Computer Engineering, University of Wisconsin–Madison, Madison, WI 53706, USA

Corresponding author: Hung Luyen (luyen@wisc.edu)

This work was supported by the Office of Naval Research (ONR) under Award N00014-16-1-2308.

ABSTRACT We describe the results of a wideband, reconfigurable reflectarray concept based on polarization-rotating unit cells (PRUCs) with a minimum-switch topology design. To enhance the simplicity and decrease the cost, the approach focuses exclusively on a one-bit phase shifting architecture. We investigated PRUCs having four conducting, single-headed arrow structures on their top surfaces and crossed, conducting strips acting as hard-wired switches on their bottom surfaces. The top-surface arrows and the bottom-surface strips are connected with four vertical vias. The switch states of the bottom conducting strips determine the two operating states of the unit cell for rotating the polarization of the reflected waves by $+90°$ and $-90°$ with respect to that of the incident, linearly polarized waves. The PRUC provides a co-polarization reflection coefficient of better than -1 dB over the wide frequency range of 8–12 GHz, as demonstrated by the simulation results. The PRUCs were incorporated into an illustrative reflectarray operating in the X-band. The full-wave simulation results show good beam scanning performance over the range of $\pm 45°$ with a maximum scan loss of 3 dB. Two static realizations of the reflectarray for beam collimation at $\theta = 0°$ and $\theta = 45°$ in the xz plane were fabricated and experimentally characterized. The measurement results show good agreement with the simulation results and demonstrate the beam steering operation of the proposed reflectarray.

INDEX TERMS Antenna arrays, beam scanning, periodic structures, reflectarray antennas, polarization rotation.

I. INTRODUCTION

Reflectarray antennas have gained significant interest in recent years as promising alternatives to conventional reflector and phased-array antennas for various wireless communication and radar applications [1]. A reflectarray collimates waves radiated from a feed antenna by having each array element scatter the waves with a specific phase shift to provide a desired phase profile for the reflected wave over the array's aperture. It is desirable for the array elements to cover a large phase range, ideally 360°, so that the reflectarray can collimate the beam while being implemented on a flat surface or conforming to an arbitrary surface topology of interest as demanded by specific applications. While having lower profiles and lighter weights than conventional parabolic reflectors, early developed reflectarrays suffered from narrow bandwidths over which the array elements could realize a large phase range [2]–[4]. Various solutions have been presented to enhance bandwidths of reflectarrays, including stacking multiple resonators together [5]–[7], utilizing subwavelength elements [8], [9], and using true-time delay unit cells [10], [11]. As demand for higher data throughputs is growing for modern wireless systems, a great deal of effort has been made to design tunable versions of array elements so that reflectarray antennas can provide adaptive pattern forming and beam scanning. While active phased arrays are considered top performers regarding the ability to synthesize a large range of radiation characteristics and adapt the radiation patterns in real time, they face several technical and practical challenges. These challenges include

The associate editor coordinating the review of this manuscript and approving it for publication was Mohsen Khalily.

high cost of transmit/receive modules, thermal management of the array for high-power applications, and low efficiencies due to losses (especially at milimeter-wave frequencies) of the feed networks and phase shifters [1]. On the other hand, reflectarrays have potential advantages of lower costs, higher power handling capabilities, as well as higher efficiencies compared to active phased arrays.

Various techniques have been presented for individual reconfiguration of phase-shifting elements of reflectarrays in numerous studies, including using mechanical movement [12], varactor diodes [13]–[15], PIN diodes [16]–[18], MEMS switches [19]–[22], as well as several tunable electromagnetic materials [23]–[25]. Reconfiguration techniques using varactor diodes, ferroelectric thin films, liquid crystals, and graphene materials have enabled adjusting the phase shift of each unit cell continuously using analog control. However, these tuning elements often produce relatively high losses in microwave frequency ranges, reducing the efficiency of the reflectarrays [1]. Additionally, the analog control requires more sophisticated architectures for voltage supply circuitry compared to those used in digital control. Reconfiguration techniques using PIN diodes and MEMS switches have been the most popular choices for microwave and milimeter-wave applications due to the maturity of these technologies. These devices are suitable for switching phase-shifting elements between discrete phase states. While a higher number of phase states results in smaller phase errors for beam collimation and better beam scanning performance, the complexity of biasing networks increases with the number of phase states. This drives significant cost increases for arrays with large numbers of elements needed for deployment in practical scenarios. Moreover, the use of additional switches and the required additional lumped elements used in their biasing networks increases the overall loss of the system. This loss compensates some of the gains achieved by using a finer phase shift discretization over the reflectarray's aperture. Therefore, reconfigurable reflectarrays using 1-bit phase correction have been of great interest due to low complexity and reduced cost. A common drawback of beam-steerable reflectarrays reported in the literature has been narrow bandwidths over which the phase-shifting elements are able to cover the 0°-360° phase range. Outside of this frequency range, the beam scanning performance of a tunable reflectarray degrades significantly, resulting in a large scan loss and limiting the scan angles. While many solutions have been proposed to enhance the bandwidths of phase-shifting elements for fixed reflectarrays [5]–[11], implementing these bandwidth enhancement features in a tunable unit cell is technically challenging. Most of reconfigurable unit cells reported to date have phase bandwidths ranging from 0.6% to 7% for a continuous phase correction [15], [16], [25]–[30] and from 0.75% to 4% for a 1-bit phase quantization [17], [18].

Recently, the concept of polarization rotation (PR) has been investigated in a few studies as a promising solution to make wideband 1-bit phase shifters for constructing reflectarrays [31]–[35]. Application of this concept for achieving wide phase bandwidths for electronically reconfigurable reflectarrays operating in Ku-band for satellite communications has been demonstrated in [31]–[33]. In [31], a numerical study was presented to demonstrate a polarization rotating unit cell (PRUC) that is reconfigured by using two anti-parallel PIN diodes and provides 1-bit phase resolution over a wide bandwidth of about 50%. A slight variation of this unit cell was later used to design an electronically beam-steerable reflectarray antenna with a wide operating bandwidth of 30%, as reported in [32]. However, the unit cells presented in [31] and [32] have relatively complicated structures consisting of 6 layers of dielectric substrates. Additionally, 16 blind via holes are required to make lateral walls for a cylindrical cavity in each unit cell, resulting in high fabrication cost and increased complexity of the reflectarray. A relatively simpler design for electronically switchable PRUCs was proposed in [33] and was demonstrated to have a 20% bandwidth of 1-bit phase resolution. However, this unit cell needs to use 4 PIN diodes for reconfiguration instead of 2 PIN diodes required for the ones presented in [31] and [32]. This increases the cost for implementing switching operation and control circuit for the reflectarray. Therefore, new PRUC designs that allow for creating electronically reconfigurable 1-bit phase shifters over a wide frequency range for reflectarrays and reducing the complexity and fabrication cost of control circuits are highly desirable.

This paper presents a PRUC topology that can be applied to design 1-bit reflectarays capable of beam scanning operation over a wide frequency range. The PRUC consists of four conducting single-headed arrow structures that are pointed towards the four corners of the unit cell and placed above a ground plane. The four diagonal strips of the arrows are connected to four vertical vias that go through four slots in the ground plane to the bottom side of the structure where a metal strip along either one of two diagonal lines is used to connect two of the four vias. The unit cell has two modes of operation corresponding to two positions of the metal strip on its bottom surface. Switching the bottom surface strip between the two positions can be done by using two single-pole single-throw (SPST) switches (or two PIN diodes), which will be shown as the minimum switch-topology for this class of PRUCs. In the two operating modes, the unit cell rotates the polarization of the reflected wave by 90° and −90° with respect to that of the incident wave. Simulation results show that the two modes of the unit cell exhibit good polarization rotation operation with a phase difference of 180° over the bandwidth of 8-12 GHz. The unit cell was used to design a reflectarray operating in X-band with aperture dimensions of $10\lambda \times 10\lambda$ at 10 GHz. Performance of the beam-steerable version of the array was evaluated in full-wave simulations through a series of static versions optimized for three different beam scanning scenarios at five different frequency points from 8 GHz to 12 GHz. Simulated radiation patterns of the static arrays show consistent beam shapes and radiation patterns for each beam scenario over this frequency range. Moreover, the maximum scan loss at a single frequency is 3 dB while

the maximum gain variation across all five frequencies and three beam scenarios (covering the scan range of $\pm 45°$) is 5.2 dB. We fabricated and experimentally characterized two static versions of the array corresponding to beam collimation at 10 GHz along two directions of $\theta = 0°$ and $\theta = 45°$ in the $\phi = 0°$ plane. Measurement results and simulation results show good agreement and demonstrate that the fabricated prototypes produce pencil beams at the intended directions with normalized side-lobe levels lower than -12.1 dB and polarization purity of better than 19.8 dB.

II. DESIGN AND SIMULATIONS OF THE POLARIZATION ROTATING UNIT CELL

Chen *et al.* [36] presented a PRUC design providing an extremely wide PR bandwidth of 4:1 with a relatively simple structure. This unit cell consists of a conducting double-headed arrow printed on a dielectric substrate backed by a ground plane. The ultra-wideband operation of the unit cell is achieved by combining multiple resonant modes of the V-shaped resonators (the arrowheads) and the dipole (the diagonal strip connecting the two arrowheads). This unit cell and its 90° rotated version can be used to realize two modes of operations corresponding to $+90°$ and $-90°$ rotations of polarizations of reflected waves with respect to those of incident waves. We modified this PRUC design to combine the two modes of operations into a single unit cell and accommodate a switching scheme that allows for reconfiguration.

Fig. 1 shows the topology of such a reconfigurable PRUC. In this design example, the unit cell is implemented using three Rogers RO4003C dielectric substrates bonded together by two layers of Rogers RO4450B prepregs. Two of the substrates used in this specific design are bonded together with a prepreg layer to form a single dielectric substrate with a custom thickness, which is not a standard thickness provided by the manufacturer. The unit cell consists of three metallic layers: a top layer with four single-headed arrow structures, a ground plane with four slots printed on the top surface of the bottom substrate, and a bottom layer where switching operation is performed. In the top metallic layer, the four arrowheads are pointed towards the four corners of the square-shaped unit cell. Each arrowhead is connected to a conducting strip aligned along a diagonal line of the unit cell. The diagonal strips of the arrows are connected to four vertical vias going through the four slots in the ground plane and reaching the bottom metallic layer, where a metal strip is oriented along either one of the two diagonal lines to connect two of the four vias. The four vias are labeled as 1, 2, 3, and 4 as shown in Figs. 1(b)-1(d). The unit cell is configured in bit-0 state when the two vias 1 and 3 are connected while the other two vias are left isolated (see Fig. 1(c)). Similarly, bit-1 state is enabled if the two vias 2 and 4 are connected while 1 and 3 are left open (see Fig. 1(d)).

The four vertical, through-substrate metallic vias play an important role in the PR operation of the proposed unit cell and change its behavior significantly compared to that of the unit cell design presented in [36]. Fig. 2 illustrates the

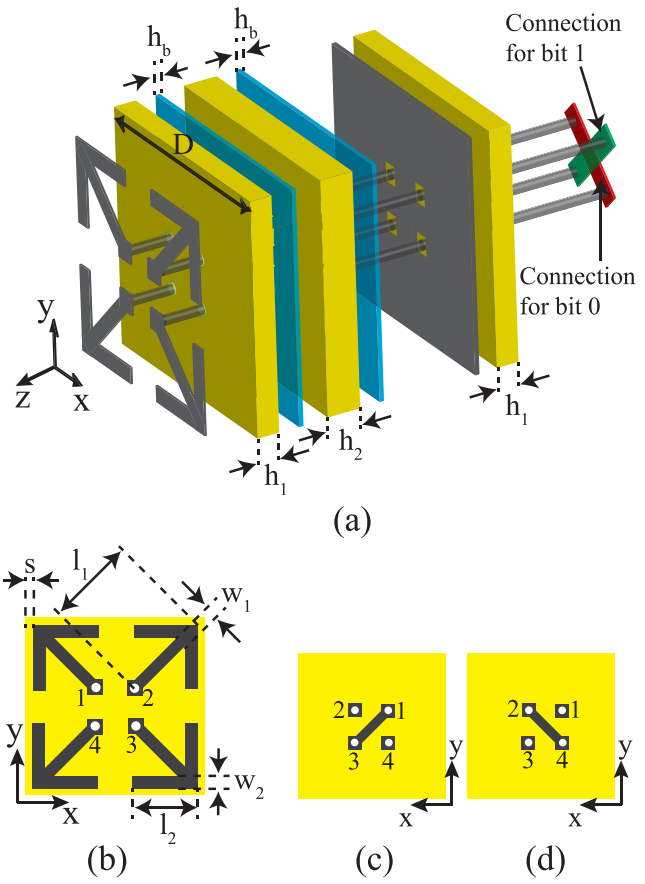

FIGURE 1. (a) Three-dimensional topology of the proposed polarization rotating unit cell with a switchable connection on the bottom side. (b) Top view of the unit cell. (c) Bottom view of the unit cell for bit-0 configuration. (d) Bottom view of the unit cell for bit-1 configuration. Dark gray represents metal, yellow represents dielectric substrates, and blue represents bonding layers.

operating principle of the proposed PRUC by showing the induced surface currents on the arrow structures and vias when the unit cell is illuminated with a $\hat{y}$-polarized incident field and configured in bit-0 and bit-1 states. In bit-0 configuration, the arrows attached to two vias 1 and 3 are connected through the bottom surface strip, extending the electrical path for the current to flow to approximately half a wavelength. This results in relatively strong currents on the bottom surface strip and lower parts of the two connected vias (1 and 3) and relatively weak currents flowing on the diagonal strips of the two connected arrows on the top metallic layer. Observe that the currents change directions near the top parts of the two connected vias (1 and 3), as shown in Fig. 2(b). Meanwhile, the other two arrows (connected to vias 2 and 4) are isolated, each of them along with their vertical via create an electrical path of approximately a quarter of a wavelength. As a result, the currents are strong on the diagonal strips of the two isolated arrows and weaker toward the open-ended vias. The unit cell acts as a PEC to reflect the component of the incident electric field parallel to the direction of the diagonal strips having strong electrical currents with a 180° phase shift while acting as a PMC to reflect the component of

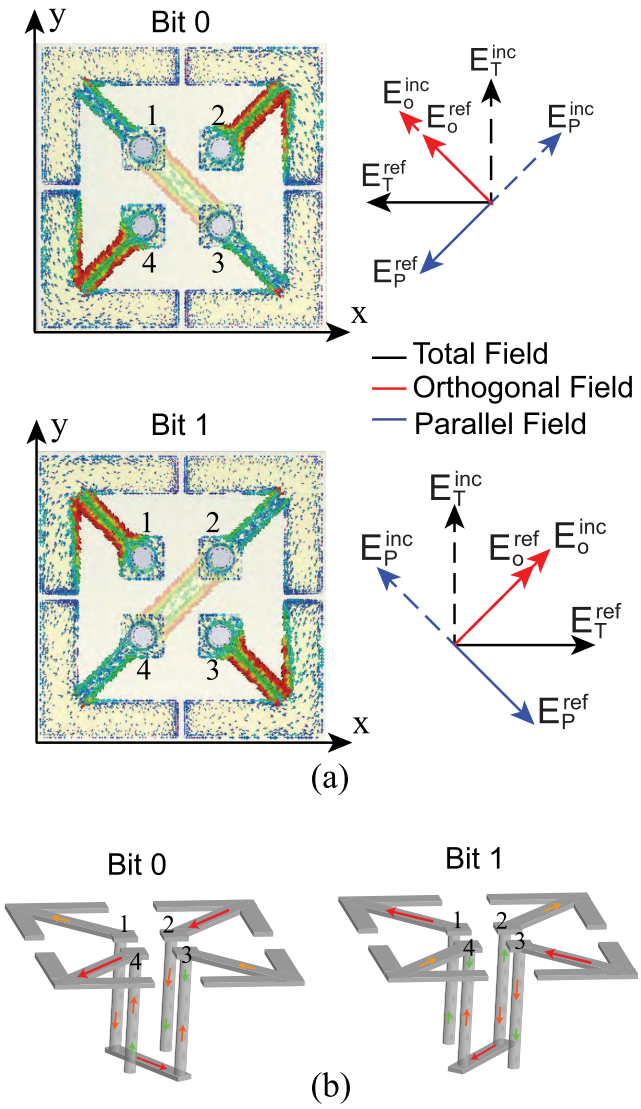

FIGURE 2. Induced surface currents on the arrows and vertical vias of the proposed PRUC in bit-0 and bit-1 configurations under illumination of an incident plane wave with a polarization along the y-axis. (a) 2-D view in the *xy* plane. (b) 3-D perspective view.

the incident electric field orthogonal to this diagonal direction with a 0° phase shift. Thus, a bit-0 unit cell produces a total reflected electric field vector pointing toward the negative $\hat{x}$–direction. In bit-1 configuration, the diagonal strips of the arrows 1 and 3 (isolated arrows) have strong currents while those of the arrows 2 and 4 (connected arrows) have weak currents. Following a similar analysis, it can be seen that the bit-1 unit cell provides the total reflected electric field vector pointing toward the positive $\hat{x}$–direction. Therefore, the bit-0 and bit-1 unit cells produce reflected electric field vectors pointing in opposite directions, which is equivalent to a phase difference of 180°. We can view the PRUC in a simplified fashion as it contains two orthogonal pairs of arrows, each of which along a diagonal line is responsible for a PR mode of the unit cell when activated. The two arrows belonging to one pair are deactivated when they are electrically connected on

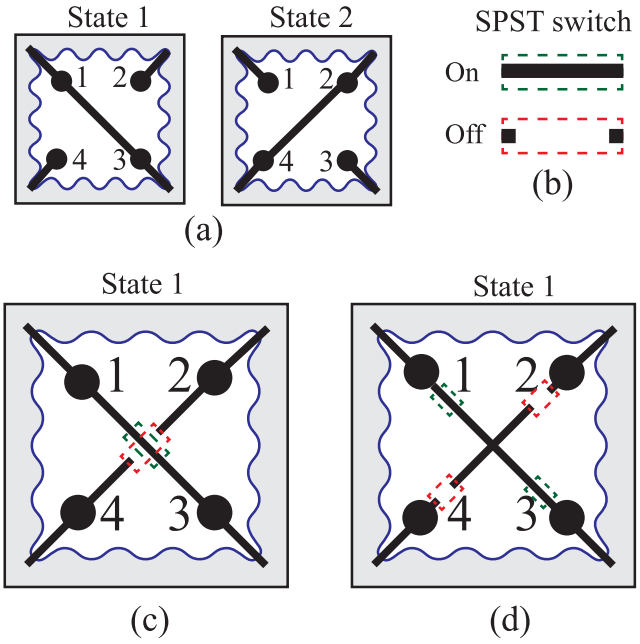

FIGURE 3. (a) Simplified functional description for two states of a generalized PRUC having similar operating principle with the PRUC proposed in this work. (b) Functional description of a SPST switch in On and Off states. (c) Example of a PRUC using two SPST switches for switching. (d) Example of a PRUC using four SPST switches for switching.

the bottom side through the vias and activated when the vias attached to them are left open.

We envision implementing a switching operation for changing the bottom surface strip between its two positions by using a double-pole double-throw (DPDT) switch or two SPST switches. With the latter option, two PIN diodes can be used to realize the function of two SPST switches to further reduce the cost of fabrication. The two PIN diodes always have opposite polarities with respect to each other (e.g., if one is forward-biased then the other one is reverse-biased and vice versa). Therefore, the two PIN diodes can use the same control signal with two opposite voltage values $+/-V$, similar to [31] and [32]. It can be shown that the minimum number of SPST switches required for switching operation for a PRUC having similar operating principle as the one presented in this work is two. The proposed unit cell is assumed to belong to a simplified, generalized class of switchable PRUCs that has two modes of polarization rotation operation. Each mode of operation of a PRUC of this class is characterized by strong induced electrical currents along one diagonal line and minimized currents along the other diagonal line of the unit cell. The direction of strong induced currents in one operating mode is orthogonal to that in the other operating mode. A functional description of a PRUC of this class is illustrated by a unit cell with four nodes (labeled as 1, 2, 3, and 4) as shown in Fig. 3(a). Currents are turned on or off along a diagonal line by connecting/disconnecting or disconnecting/connecting the two nodes along this line. Fig. 3(a) shows two states of the unit cell, namely State 1 and State 2. In State 1 (or 2), two nodes

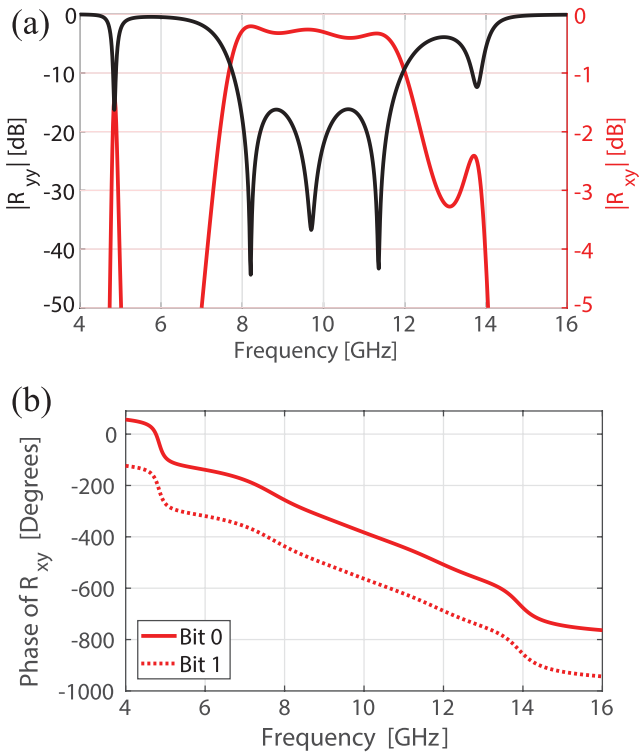

FIGURE 4. Simulated reflection coefficients of the reconfigurable PRUC. (a) Magnitudes of the co-polarization (R_{xy}) and cross-polarization (R_{yy}) reflection coefficients of the PRUC. (b) Phases of the co-polarization reflection coefficients of bit-0 and bit-1 unit cells.

1 and 3 are connected (or disconnected) while nodes 2 and 4 are disconnected (or connected). The action of connecting and disconnecting the two nodes is implemented by using an SPST switch with On and Off states shown in Fig. 3(b). It is obvious that one cannot use only one SPST switch to switch the unit cell from State 1 to State 2 and vice versa. For example, assume that the SPST switch is used to implement the short circuit (in State 1) and open circuit (in State 2) between nodes 1 and 3. To realize State 1, the nodes 2 and 4 must be disconnected. However, the nodes 2 and 4 are always disconnected since there is no switching operation performed between these two nodes. Therefore State 2, which requires the nodes 2 and 4 to be connected, cannot be realized. By adding another SPST switch to control the connection and disconnection of nodes 2 and 4, both State 1 and State 2 can be realized. Thus, the minimum number of SPST switches to perform the switching between the two states of the unit cell is two. An example of using two SPST switches to perform the switching for the unit cell is illustrated in Fig. 3(c). Another example of using four SPST switches, similar to the solution implemented in [33], is illustrated in Fig. 3(d). It should be noted that both PRUC designs proposed in our work and in [33] satisfy the description for the generalized class of PRUCs discussed in this section.

We simulated the proposed PRUC using the unit cell boundary condition in CST Microwave Studio. The periodicity of the unit cell is $D = 6$ mm, which is equivalent to a fifth of the free-space wavelength at 10 GHz. The dimensions of the proposed PR unit cell, including the width and length of the diagonal strips of the arrows, w_1 and l_1, width and length of the arrowheads, w_2 and l_2, spacing between each arrowhead and the nearest edge of the unit cell, s, and the thicknesses of the dielectric substrates, h_1 and h_2, were tuned to achieve a high co-polarization reflection coefficient from 8 to 12 GHz. While the thicknesses of the dielectric substrates were changed between standard thicknesses of Rogers RO4003C laminates provided by the manufacturer, the other parameters were more freely varied as long as the minimum feature of the unit cell is still realizable with printed circuit board (PCB) lithography. Additionally, the width of the bottom-surface metal strip acting as a hard-wired connection was chosen to be 0.5 mm, approximating to the width of a commercial PIN switch diode (e.g., MACOM MA4SPS402) that can be a potential candidate for implementing future electronically reconfigurable versions of the unit cell. Fig. 4(a) shows the simulation results for the magnitudes of the co-polarization and cross-polarization reflection coefficients, R_{xy} and R_{yy}, of an illustrative (bit-0 or bit-1) PRUC. The PRUC delivers a high co-polarization reflection coefficient ($R_{xy} > -1$ dB) and low cross-polarization reflection coefficient ($R_{yy} < -10$ dB) over the frequency range of 8-12 GHz. Fig. 4(b) shows that the bit-0 and bit-1 unit cells produce a phase difference of 180° for the co-polarization reflection coefficient in an extremely wide frequency range from 4 GHz to 16 GHz, demonstrating their suitability to act as wideband 1-bit phase shifters. The dimensions of the illustrative PRUC are listed in Table 1.

TABLE 1. Dimensions of the illustrative PRUC.

w_1	l_1	w_2	l_2	s	h_1	h_2
0.25	2.6	0.7	2.75	0.15	0.81	1.52

All dimensions are in mm.

Table 2 compares the illustrative PRUC presented in this work with those reported previously in [31]–[33] regarding several key parameters. Compared to the PRUC designs presented in [31]–[33], the PRUC proposed in this paper uses fewer dielectric layers and has a significantly smaller number of drilled holes, allowing for reducing the fabrication cost of an array comprising a large number of phase shifting elements. Additionally, this PRUC needs two PIN diodes for reconfiguration, similar to the unit cell presented in [31] and [32], which is half of the number of PIN diodes required for the unit cell reported in [33]. It is desirable to use as few PIN diodes as possible for a reconfigurable reflectarray for further cost reduction since PIN diodes are relatively expensive compared to other lumped components that may be used in a control circuitry. While offering reduced complexity, the proposed PRUC provides a simulated fractional bandwidth, defined as the relative frequency range over which the co-polarization reflection coefficient is higher than -1 dB, of 42% which is larger than the values estimated for the unit cells in [31] (37%) and [33] (22%).

TABLE 2. Comparison of PRUCs acting as 1-bit phase shifters reported in different works.

Reference	[31] & [32]	[33]	**This work**
Bandwidth	10-14.5 GHz (37%)	11.9-14.8 GHz (22%)	**7.8-12 GHz (42%)**
N° of substrates	5	4	**3**
N° of drilled holes*	17	17	**4**
N° of PIN diodes	2	4	**2**

* Including metalized vias and non-metalized through holes.

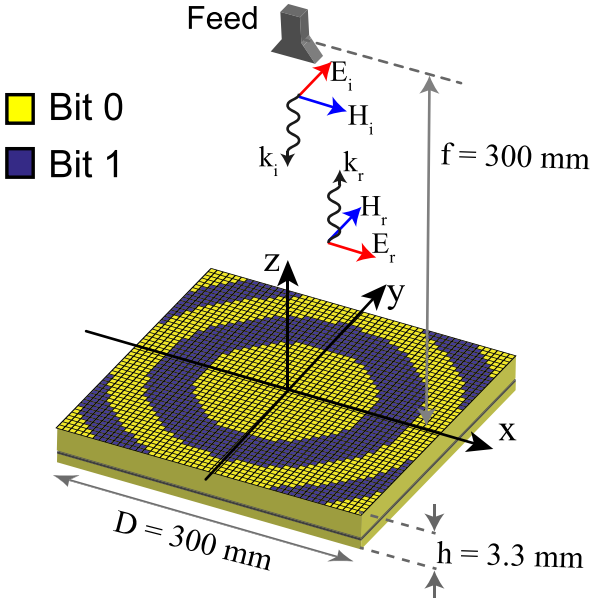

FIGURE 5. Configuration of the 1-bit reflectarray antenna.

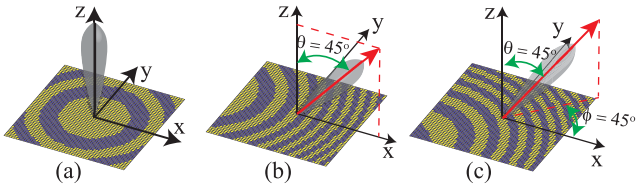

FIGURE 6. Patterns of 1-bit phase shifters on the reconfigurable reflectarray for three beam scanning scenarios where the main beams are at (a) $\theta_0 = 0°$, (b) $\theta_0 = 45°$ in the $\phi = 0°$ plane, and (c) $\theta_0 = 45°$ in the $\phi = 45°$ plane.

III. DESIGN AND SIMULATIONS OF THE BEAM-STEERABLE, 1-BIT REFLECTARRAY

The reconfigurable PRUC with ideal switching operation presented in the previous section was used to construct a prototype beam-steerable reflectarray utilizing 1-bit phase correction. Fig. 5 shows the configuration of this reflectarray antenna. The reflectarray has aperture dimensions of 300×300 mm^2, equivalent to $10\lambda \times 10\lambda$ where λ is the free-space wavelength at 10 GHz. A custom-made feed horn antenna constructed from aluminum with an aperture area of 40×40 mm^2 was placed at a focal distance of 300 mm away from the reflectarray. Full-wave simulations of the feed horn antenna (without the reflectarray) were conducted using

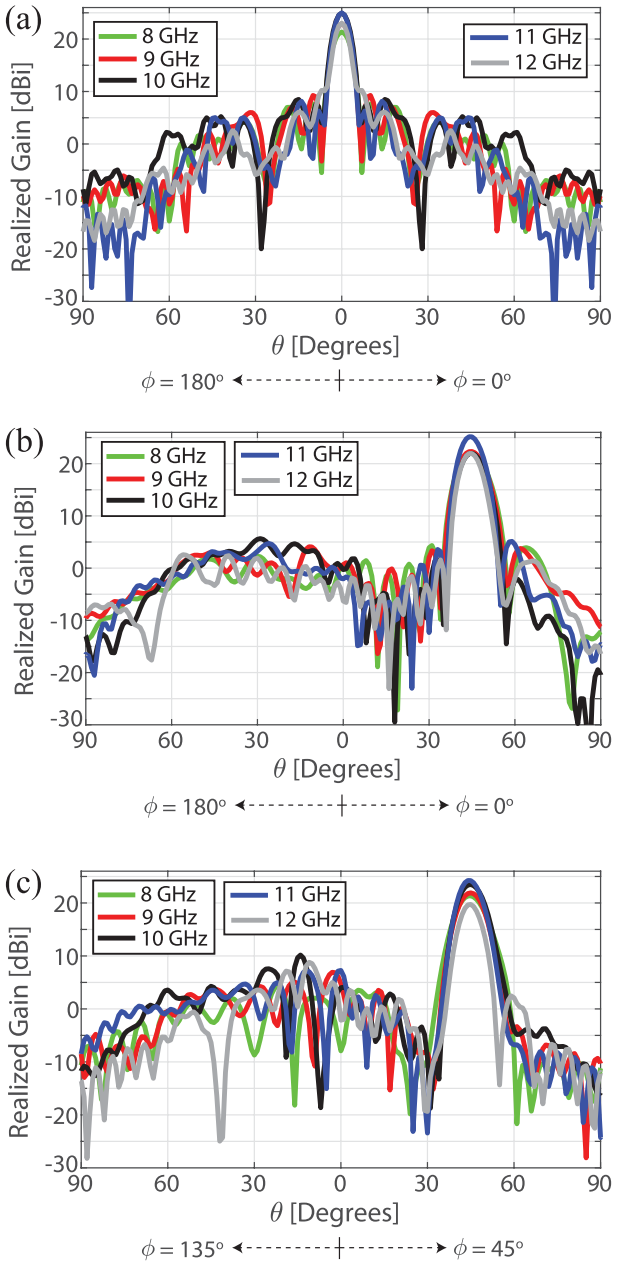

FIGURE 7. Simulated co-polarized radiation patterns of the reconfigurable reflectarray antenna at 8 GHz, 9 GHz, 10 GHz, 11 GHz, and 12 GHz for three beam scanning scenarios where the main beams are at (a) $\theta_0 = 0°$, (b) $\theta_0 = 45°$ in the $\phi = 0°$ plane, and (c) $\theta_0 = 45°$ in the $\phi = 45°$ plane.

CST Microwave Studio to compute the phase and amplitude distribution of the incident electric field generated by the feed antenna on the surface coinciding the reflectarray aperture. The amplitude tapering of the incident field at 10 GHz is -5.7 dB, -9.6 dB, and -12.3 dB at the edges of the aperture along the x–, y–, and diagonal directions, respectively [34]. The extracted phase distribution of the incident electric field was then used to configure the Fresnel patterns of the reconfigurable reflectarray antenna for beam collimation at three different directions: $\theta_0 = 0°$, $\theta_0 = 45°$ in the $\phi = 0°$ plane

(E–plane), and $\theta_0 = 45°$ in the $\phi = 45°$ plane (D–plane). For each beam scanning scenario, the phase-shifter patterns of the reflectarray were optimized at 5 different frequency points from 8 GHz to 12 GHz with a 1 GHz increment. A Fresnel pattern was derived, following the procedure presented in [34], for each combination of beam scenario and frequency. This Fresnel pattern was then represented as a binary string to act as one individual of the initial population (consisting of 50 individuals) for a genetic algorithm (GA) optimization, which was deployed to further optimize the pattern of the 1-bit phase shifters for enhancing the maximum realized gain produced by the reflectarray antenna. While the GA optimization resulted in a gain enhancement of 0.5 dB for the beam collimation at broadside direction, it did not provide any significant increase in the maximum realized gains for the other two beam scanning scenarios. The optimized patterns of the 1-bit phase shifters of the reflectarray for the three beam scanning scenarios at 10 GHz are shown in Fig. 6.

We conducted full-wave simulations of the complete model of the reflectarray and feed horn antenna to predict its performance in the three different beam scanning scenarios and five frequency points. There are a total of 15 static versions of the reflectarray antenna evaluated in the simulations, each version corresponds to a combination of beam scenario and frequency. Figs. 7(a)-7(c) show the simulated realized gain patterns for the co-polarization components of the field radiated by the reflectarray antenna in the three beam scanning scenarios where the main beams are at $\theta_0 = 0°, \theta_0 = 45°$ in the $\phi = 0°$ plane (E–plane), and $\theta_0 = 45°$ in the $\phi = 45°$ plane, respectively. In each figure, the patterns for the five frequency points from 8 GHz to 12 GHz are plotted on top of each other for direct comparison. Overall, the reflectarray provides consistent beam shapes and radiation patterns across this frequency range for all three beam scenarios. For each beam scanning scenario, the main beams are created exactly at the desired direction. The side-lobe levels, normalized to the respective main-lobe levels, are less than -13 dB for the first beam scenario ($\theta_0 = 0°$), less than -17 dB for the second beam scenario ($\theta_0 = 45°$ in the $\phi = 0°$ plane), and less than -14 dB for the third beam scenario ($\theta_0 = 45°$ in the $\phi = 45°$ plane). Fig. 8 shows the maximum realized gain provided by the reconfigurable reflectarray as a function of frequency for the three beam scanning scenarios. The maximum realized gain for the reflectarray antenna reaches 25 dBi for the first two beam scenarios and 24.1 dBi for the third beam scenario at 11 GHz. The maximum realized gain values vary within 3.6 dB, 3.1 dB, and 4.3 dB for beam collimation at $\theta_0 = 0°, \theta_0 = 45°$ in the $\phi = 0°$, and $\theta_0 = 45°$ in the $\phi = 45°$ plane, respectively, over the frequency range of 8-12 GHz. The gain drop across different beam scanning scenarios is about 0.7 dB at 8 GHz, 1 dB at 9 GHz, 3 dB at 10 GHz, 0.8 dB at 11 GHz, and 3 dB at 12 GHz.

IV. EXPERIMENTAL RESULTS

We fabricated two static versions of the reflectarray corresponding to beam collimation at $\theta_0 = 0°$ and $\theta_0 = 45°$ in

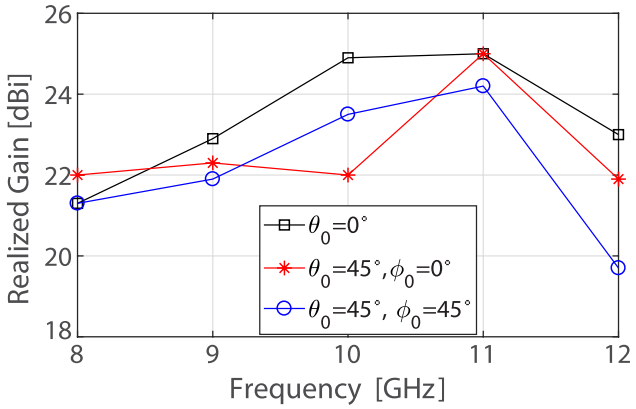

FIGURE 8. Simulated maximum realized gains of the reconfigurable reflectarray at 8 GHz, 9 GHz, 10 GHz, 11 GHz, and 12 GHz for the three beam scanning scenarios.

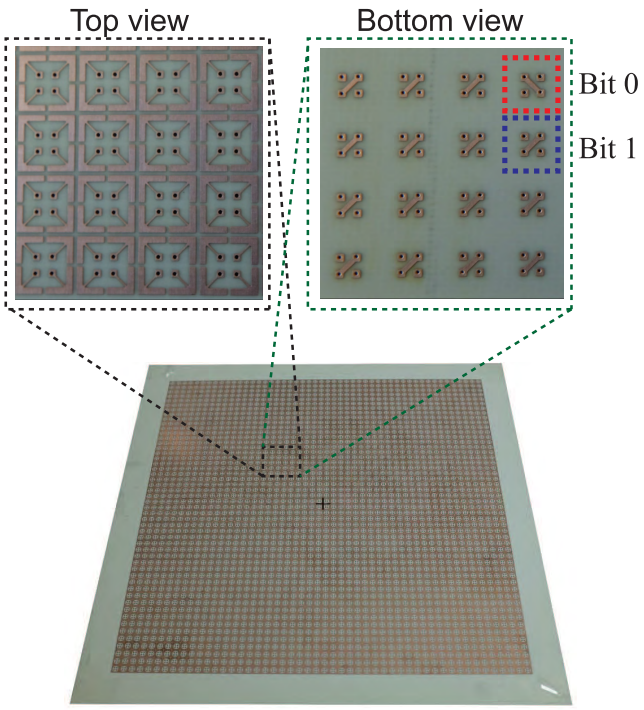

FIGURE 9. Photograph of a fabricated static prototype of the reflectarray.

the $\phi = 0°$ plane at 10 GHz. Each prototype was fabricated using PCB lithography and implemented on three Rogers RO4003C substrates bonded together by two layers of Rogers RO4450B. The total thickness of each fabricated array prototype is about 3.3 mm. The vertical vias connecting the top metallic layer with the bottom metallic layer were implemented with plated via holes with diameters of 0.46 mm. The connections on the bottom metallic layer representing ideal switching function were implemented by fixed copper traces with widths of 0.5 mm. Fig. 9 shows a photograph of a fabricated static array prototype along with the zoom-in views for the top and bottom surfaces of the array. The top metallic layer of all unit cells are the same while the copper traces for

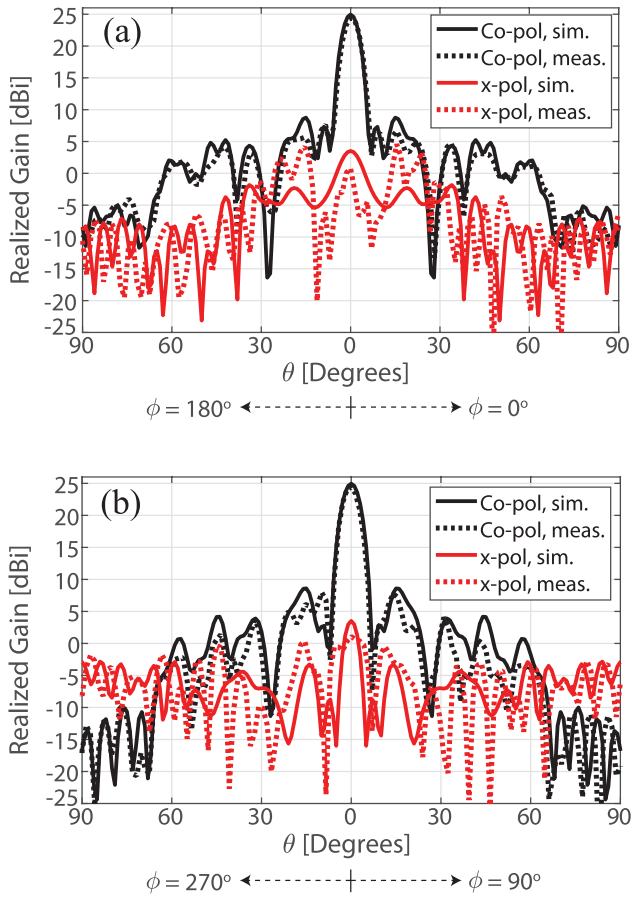

FIGURE 10. Measured and simulated radiation patterns of the static version of the reflectarray antenna for beam collimation at broadside direction at 10 GHz in the (a) E–plane (*xy* plane) and (b) H–plane (*yz* plane).

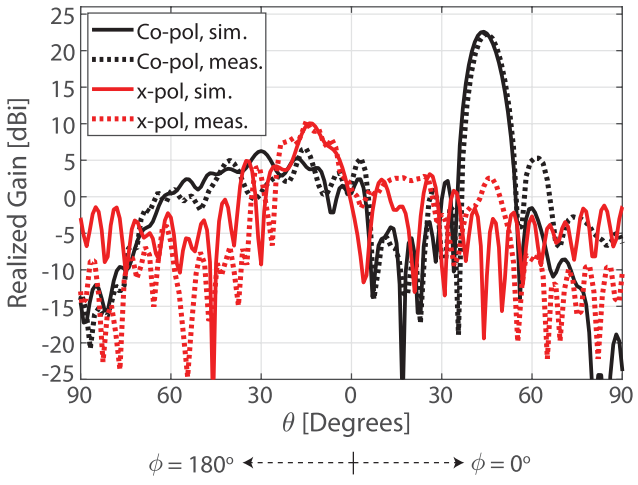

FIGURE 11. Measured and simulated radiation patterns of the static version of the reflectarray antenna for beam collimation at $\theta_0 = 45°$ in the *xz* plane at 10 GHz.

electrical connection on the bottom side are orthogonal for bit-0 and bit-1 configurations.

The two fabricated static prototypes were characterized using a near-field spherical measurement system. A styrofoam fixture was used to position the reflectarrays and the feed antenna during the measurements. Radiation patterns of each prototype were measured at the intended operating frequency of 10 GHz. Figs. 10(a) and 10(b) show the measurement results along with the simulation results for the co-polarization and cross-polarization patterns in the E– and H–planes of the fabricated prototype providing beam collimation at broadside direction. The measured realized gain at the broadside direction of this static prototype is 24.4 dBi, corresponding to an aperture efficiency of 21.9%. These measured gain and aperture efficiency are slightly lower than the simulated values of 25 dBi and 25.1%, respectively. However, the directivity values of this static prototype are the same and equal to 25.3 dBi in both the measurement and simulation. The fabricated prototype provides a slightly lower side-lobe level (−16.8 dB in the measurement vs. −16.2 dB in the simulation) and higher polarization purity in the direction of the main beam (23.7 dB in the measurement vs. 21.5 dB in the simulation) compared to the values predicted in the full-wave simulations in the E–plane. The discrepancies between the measurement and simulation results for the side-lobe and cross-polarization levels in the H–plane are slightly smaller than those in the E–plane. Fig. 11 shows the measurement and simulation results for the radiation patterns of the fabricated prototype for beam collimation at $\theta_0 = 45°$ in the $\phi = 0°$ plane. The fabricated prototype generates a main beam at $\theta = 45°$ as predicted in the simulations. The maximum realized gain and normalized side-lobe level acquired in the measurements are 22.3 dBi and −12.1 dB, respectively, which agree quite well with the simulated values (maximum realized gain of 22.6 dBi and normalized side-lobe level of −12.5 dB). The measured directivity of the fabricated prototype is 22.9 dBi, showing reasonable agreement with the predicted value of 23.2 dBi. The aperture efficiency for this static prototype is 13.5% in the measurement and 14.4% in the simulation. Noticeable differences between the measurement and simulation results can be seen regarding the cross-polarization level in the direction of the main beam and the side-lobe level immediately on the right hand side of the main lobe. While these levels are higher in the measurements compared to the simulations, the fabricated prototype still provides a very good polarization purity of 19.8 dB in the direction of the main beam and a relatively low normalized level of −17 dB for the first right-hand side-lobe. These discrepancies can be attributed to fabrication tolerances, measurement uncertainties, features in measurement setup that were not taken into account in the full-wave simulations (e.g. the styrofoam fixture, cable connecting the feed horn and the test port of the measurement chamber), and possible positioning errors of the feed horn with respect to the reflectarray.

V. CONCLUSION

We presented a polarization-rotating unit cell that can act as a wideband 1-bit spatial phase shifter for reconfigurable reflectarray antennas. The PRUC consists of three metallic layers separated by dielectric substrates. The top metallic layer

includes two pairs of single-headed arrow structures pointing towards the four corners of the square-shaped unit cell. Four diagonal strips of these arrow structures are connected to four vertical via holes going through the slots in the ground plane (as the middle metallic layer) and extending to the bottom metallic layer. In the bottom metallic layer, a metallic strip is used to connect two of the four via holes along either one of the two diagonal directions, enabling either bit-0 or bit-1 configuration for the PRUC. This metallic strip acts as a hard-wired connection, which should be replaced with an electronically-switchable element such as a PIN diode in the electronically-switchable versions of this design. Depending on the electrical connection in the bottom metallic layer, the unit cell activates two arrows along a diagonal line while deactivating the other two arrows along the other diagonal line for polarization rotation operation. The two polarization rotation modes of the unit cell result in rotations of the reflected electric field vector by $+90°$ and $-90°$ with respect to the incident electric field vector, creating a phase difference of 180° in the reflected field between the two modes over an extremely wide frequency range. The PRUC demonstrates a high co-polarization reflection coefficient ($|R_{xy}| > -1$ dB) over the frequency range from 8-12 GHz as shown by the simulation results. This enables the reconfiguration of a reflectarray over a very wide bandwidth when the PRUCs are used as 1-bit phase shifters for the array.

The PRUC was used as a building block for a reconfigurable reflectarray with aperture dimensions of $10\lambda \times 10\lambda$, where λ is the free-space wavelength at 10 GHz. We simulated 15 static versions of the array optimized for beam collimation along three different directions ($\theta_0 = 0°$, $\theta_0 = 45°$ in the $\phi = 0°$ plane, and $\theta_0 = 45°$ in the $\phi = 45°$ plane) at five different frequencies (8, 9, 10, 11, and 12 GHz) to evaluate beam scanning performance of the array. Simulation results demonstrate good beam scanning performance in the range of $\pm 45°$ with a maximum gain variation of 5.2 dB over the frequency range of 8-12 GHz. Two static versions corresponding to beam collimation at $\theta_0 = 0°$ and $\theta_0 = 45°$ in the $\phi = 0°$ plane at 10 GHz were fabricated and their radiation patterns were measured. Measurement results show that the fabricated prototypes provide pencil beams at $\theta_0 = 0°$ and $\theta_0 = 45°$ with the realized gains of 24.4 dBi and 22.3 dBi, respectively, while having relatively low side lobe levels (< -12 dB) and high polarization purity (> 19 dB). The measurement results agree quite well with the simulation results for the two prototypes, demonstrating the scanning performance of the proposed reflectarray and validity of using the presented PRUC as wideband 1-bit spatial phase shifters for reconfigurable reflectarrays. While a more realistic switch for reconfiguring the PRUC has not been taken into account for these proof-of-concept demonstrations, we envision that the switching mechanism can be implemented electronically using commercially available DPDT switches, SPST switches, or PIN diodes. The proposed PRUC would need 2 PIN diodes (or 2 SPST switches) to perform the switching, which was shown to be the minimum-switch topology for this class of PRUCs. Further study on deploying the fully tunable version of the reflectarray using electronically reconfigurable PR unit cells is warranted.

REFERENCES

[1] S. V. Hum and J. Perruisseau-Carrier, "Reconfigurable reflectarrays and array lenses for dynamic antenna beam control: A review," *IEEE Trans. Antennas Propag.*, vol. 62, no. 1, pp. 183–198, Jan. 2014.
[2] D. M. Pozar, S. D. Targonski, and H. D. Syrigos, "Design of millimeter wave microstrip reflectarrays," *IEEE Trans. Antennas Propag.*, vol. 45, no. 2, pp. 287–296, Feb. 1997.
[3] D. M. Pozar, "Bandwidth of reflectarrays," *Electron. Lett.*, vol. 39, no. 21, pp. 1490–1491, Oct. 2003.
[4] M. Bozzi, S. Germani, and L. Perregrini, "Performance comparison of different element shapes used in printed reflectarrays," *IEEE Antennas Wireless Propag. Lett.*, vol. 2, no. 1, pp. 219–222, 2003.
[5] E. Carrasco, M. Barba, J. A. Encinar, M. Arrebola, F. Rossi, and A. Freni, "Design, manufacture and test of a low-cost shaped-beam reflectarray using a single layer of varying-sized printed dipoles," *IEEE Trans. Antennas Propag.*, vol. 61, no. 6, pp. 3077–3085, Jun. 2013.
[6] M. Rafaei-Booket, Z. Atlasbaf, and M. Shahabadi, "Broadband reflectarray antenna on a periodically perforated substrate," *IEEE Trans. Antennas Propag.*, vol. 64, no. 8, pp. 3711–3717, Aug. 2016.
[7] S.-W. Qu, H.-X. Zhang, W.-W. Wu, P.-F. Li, S. Yang, and Z.-P. Nie, "Wideband folded reflectarray using novel elements with high orthogonal polarization isolation," *IEEE Trans. Antennas Propag.*, vol. 64, no. 7, pp. 3195–3200, Jul. 2016.
[8] P. Nayeri, F. Yang, and A. Z. Elsherbeni, "Broadband reflectarray antennas using double-layer subwavelength patch elements," *IEEE Antennas Wireless Propag. Lett.*, vol. 9, pp. 1139–1142, 2010.
[9] A. Edalati and K. Sarabandi, "Wideband reflectarray antenna based on miniaturized element frequency selective surfaces," in *Proc. Eur. Conf. Antennas Propag. (EuCAP)*, Mar. 2012, pp. 362–364.
[10] E. Carrasco, J. A. Encinar, and M. Barba, "Bandwidth improvement in large reflectarrays by using true-time delay," *IEEE Trans. Antennas Propag.*, vol. 56, no. 8, pp. 2496–2503, Aug. 2008.
[11] S. M. A. M. H. Abadi, K. Ghaemi, and N. Behdad, "Ultra-wideband, true-time-delay reflectarray antennas using ground-plane-backed, miniaturized-element frequency selective surfaces," *IEEE Trans. Antennas Propag.*, vol. 63, no. 2, pp. 534–542, Feb. 2015.
[12] X. Yang *et al.*, "A broadband high-efficiency reconfigurable reflectarray antenna using mechanically rotational elements," *IEEE Trans. Antennas Propag.*, vol. 65, no. 8, pp. 3959–3966, Aug. 2017.
[13] S. V. Hum, M. Okoniewski, and R. J. Davies, "Realizing an electronically tunable reflectarray using varactor diode-tuned elements," *IEEE Microw. Wireless Compon. Lett.*, vol. 15, no. 6, pp. 422–424, Jun. 2005.
[14] O. G. Vendik and M. Parnes, "A phase shifter with one tunable component for a reflectarray antenna," *IEEE Antennas Propag. Mag.*, vol. 50, no. 4, pp. 53–65, Aug. 2008.
[15] L. Boccia, G. Amendola, and G. D. Massa, "Performance improvement for a varactor-loaded reflectarray element," *IEEE Trans. Antennas Propag.*, vol. 58, no. 2, pp. 585–589, Feb. 2010.
[16] S. V. Hum, M. Okoniewski, and R. J. Davies, "Modeling and design of electronically tunable reflectarrays," *IEEE Trans. Antennas Propag.*, vol. 55, no. 8, pp. 2200–2210, Aug. 2007.
[17] H. Kamoda, T. Iwasaki, J. Tsumochi, T. Kuki, and O. Hashimoto, "60-GHz electronically reconfigurable large reflectarray using single-bit phase shifters," *IEEE Trans. Antennas Propag.*, vol. 59, no. 7, pp. 2524–2531, Jul. 2011.
[18] H. Yang *et al.*, "A 1-bit 10×10 reconfigurable reflectarray antenna: Design, optimization, and experiment," *IEEE Trans. Antennas Propag.*, vol. 64, no. 6, pp. 2246–2254, Jun. 2016.
[19] B. Wu, A. Sutinjo, M. E. Potter, and M. Okoniewski, "On the selection of the number of bits to control a dynamic digital MEMS reflectarray," *IEEE Antennas Wireless Propag. Lett.*, vol. 7, pp. 183–186, Mar. 2008.
[20] J. Perruisseau-Carrier and A. K. Skriverviky, "Monolithic MEMS-based reflectarray antenna cell digitally reconfigurable over a 360° phase range, *IEEE Antennas Wireless Propag. Lett.*, vol. 7, pp. 138–141, 2008.
[21] H. Rajagopalan, Y. Rahmat-Samii, and W. A. Imbriale, "RF MEMS actuated reconfigurable reflectarray patch-slot element," *IEEE Trans. Antennas Propag.*, vol. 56, no. 12, pp. 3689–3699, Dec. 2008.

[22] T. Debogovic and J. Perruisseau-Carrier, "Low loss MEMS-reconfigurable 1-bit reflectarray cell with dual-linear polarization," *IEEE Trans. Antennas Propag.*, vol. 62, no. 10, pp. 5055–5060, Oct. 2014.
[23] E. Carrasco and J. Perruisseau-Carrier, "Reflectarray antenna at terahertz using graphene," *IEEE Antennas Wireless Propag. Lett.*, vol. 12, pp. 253–256, 2013.
[24] E. Carrasco, M. Tamagnone, and J. Perruisseau-Carrier, "Tunable graphene reflective cells for THz reflectarrays and generalized law of reflection," *Appl. Phys. Lett.*, vol. 102, no. 10, 2013, Art. no. 104103.
[25] G. Perez-Palomino *et al.*, "Design and experimental validation of liquid crystal-based reconfigurable reflectarray elements with improved bandwidth in F-band," *IEEE Trans. Antennas Propag.*, vol. 61, no. 4, pp. 1704–1713, Apr. 2013.
[26] M. Riel and J.-J. Laurin, "Design of an electronically beam scanning reflectarray using aperture-coupled elements," *IEEE Trans. Antennas Propag.*, vol. 55, no. 5, pp. 1260–1266, May 2007.
[27] C. Liu and S. V. Hum, "An electronically tunable single-layer reflectarray antenna element with improved bandwidth," *IEEE Antennas Wireless Propag. Lett.*, vol. 9, pp. 1241–1244, 2010.
[28] F. Venneri, S. Costanzo, and G. Di Massa, "Design and validation of a reconfigurable single varactor-tuned reflectarray," *IEEE Trans. Antennas Propag.*, vol. 61, no. 2, pp. 635–645, Feb. 2013.
[29] S. Costanzo, F. Venneri, A. Raffo, G. Di Massa, and P. Corsonello, "Radial-shaped single varactor-tuned phasing line for active reflectarrays," *IEEE Trans. Antennas Propag.*, vol. 64, no. 7, pp. 3254–3259, Jul. 2016.
[30] S. Costanzo, F. Venneri, G. Di Massa, A. Borgia, and A. Raffo, "Bandwidth performances of reconfigurable reflectarrays: State of art and future challenges," *Radioengineering*, vol. 27, no. 1, pp. 1–9, 2018.
[31] S. Montori *et al.*, "Wideband dual-polarization reconfigurable elementary cell for electronic steerable reflectarray at Ku-band," in *Proc. 4th Eur. Conf. Antennas Propag. (EuCAP)*, Apr. 2010, pp. 1–5.
[32] S. Montori *et al.*, "A transportable reflectarray antenna for satellite ku-band emergency communications," *IEEE Trans. Antennas Propag.*, vol. 63, no. 4, pp. 1393–1407, Apr. 2015.
[33] M.-T. Zhang *et al.*, "Design of novel reconfigurable reflectarrays with single-bit phase resolution for Ku-band satellite antenna applications," *IEEE Trans. Antennas Propag.*, vol. 64, no. 5, pp. 1634–1641, May 2016.
[34] H. Luyen, Z. Yang, M. Gao, J. H. Booske, and N. Behdad, "A wideband, single-layer reflectarray exploiting a polarization rotating unit cell," *IEEE Trans. Antennas Propag.*, vol. 67, no. 2, pp. 872–883, Feb. 2019.
[35] H. Luyen, K. Mavrakakis, J. H. Booske, and N. Behdad, "Wideband reflectarray and transmitarray designs using polarization rotating unit cells," in *Proc. 18th Int. Symp. Antenna Tech. Appl. Electromagn. (ANTEM)*, Waterloo, ON, USA, Aug. 2018, pp. 1–3.
[36] H. Chen *et al.*, "Ultra-wideband polarization conversion metasurfaces based on multiple plasmon resonances," *J. Appl. Phys.*, vol. 115, no. 15, Apr. 2014, Art. no. 154504.

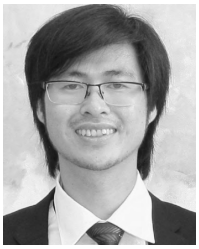

HUNG LUYEN (S'13–M'17) received the B.E. degree in electrical engineering from the Hanoi University of Technology, Vietnam, in 2010, and the M.S. and Ph.D. degrees in electrical engineering from the University of Wisconsin–Madison, Madison, WI, USA, in 2014 and 2017, respectively.

He is currently a Postdoctoral Researcher with the Department of Electrical and Computer Engineering, University of Wisconsin–Madison. His research interests include antenna design, applied electromagnetics, and medical applications of microwaves. He received the Vietnam Education Foundation Fellowship, in 2012, and was an honorable mention, in 2013, and a finalist, in 2014, in the Student Paper Competition of the IEEE International Symposium on Antennas and Propagation and USNC/URSI National Radio Meeting.

ZONGTANG ZHANG (S'18) received the B.Sc. degree in applied physics from Xidian University, Xi'an, China, in 2014, and the M.S. degree in applied physics from the University of Electronic Science and Technology of China, Chengdu, China, in 2017. He is currently pursuing the Ph.D. degree in electrical engineering with the University of Wisconsin–Madison, Madison, WI, USA.

Since 2017, he has been a Research Assistant with the Department of Electrical and Computer Engineering, University of Wisconsin–Madison. His research interests include multiband antennas, periodic structures, frequency selective surfaces, and phased-array antennas.

JOHN H. BOOSKE (S'82–M'85–SM'93–F'07) received the Ph.D. degree in nuclear engineering from the University of Michigan, Ann Arbor, MI, USA, in 1985.

From 1985 to 1989, he was a Research Scientist with the University of Maryland, College Park, MD, USA, researching magnetically confined hot ion plasmas and sheet-electron-beam free-electron lasers. From 2001 to 2005, he served as the Director of the UW Interdisciplinary Materials Science Program. Since 1990, he has been a Faculty Member with the Department of Electrical and Computer Engineering, University of Wisconsin–Madison (UW), which he chaired, from 2009 to 2018. Currently he is the Director of the Wisconsin Collaboratory for Enhanced Learning and also the Duane H. and Dorothy M. Bluemke Professor of Engineering and the UW-Madison Vilas Distinguished Achievement Professor. He was a Co-Editor of the *Microwave and Radio Frequency Applications* (American Ceramic Society, in 2003) and *Microwave and Millimeter-Wave Power Electronics* (the IEEE/Wiley, in 2005). His research interests include experimental and theoretical study of coherent electromagnetic radiation, its sources, and its applications, spanning the RF, microwave, millimeter-wave, and THz regimes. His recent research activities include vacuum electronics, microfabrication of millimeter-wave and THz regime sources and components, high-power microwaves, advanced cathodes, physics of the interaction of THz radiation and materials, microwave-generated plasma discharges, electromagnetic metamaterials, and biological applications of electric and electromagnetic fields.

Dr. Booske is a Fellow of the American Physical Society, in 2011. He has received many teaching awards, including the UW Chancellor's Distinguished Teaching Award, the UW Teaching and Learning Innovation Award, and the IEEE EAB Major Educational Innovation Award. In 2018, he received the IEEE Plasma Science and Applications Prize Award. He received the University of Wisconsin Vilas Associate Award for research and the U.S. National Science Foundation Presidential Young Investigator Award. He has been a Guest Editor of the IEEE TRANSACTIONS ON PLASMA SCIENCE.

NADER BEHDAD (S'98–M'06–SM'12–F'17) received the B.S. degree in electrical engineering from the Sharif University of Technology, Tehran, Iran, in 2000, and the M.S. and Ph.D. degrees in electrical engineering from the University of Michigan, Ann Arbor, MI, USA, in 2003 and 2006, respectively.

From 2006 to 2008, he was an Assistant Professor with the Electrical Engineering and Computer Science Department, University of Central Florida, Orlando, FL, USA. From 2009 to 2013, he was an Assistant Professor with the Electrical and Computer Engineering Department, University of Wisconsin–Madison, Madison, WI, USA, where he was an Associate Professor, from 2013 to 2016. He is currently a Professor with the Department of Electrical and Computer Engineering and the Harvey D. Spangler Faculty Scholar with the College of Engineering, University of Wisconsin–Madison. His current research interests include applied electromagnetics, electrically small antennas, antenna arrays, antennas for biomedical applications, biomedical applications of RF/microwaves, periodic structures, frequency selective surfaces, passive high-power microwave devices, metamaterials, and biomimetics and biologically inspired systems in electromagnetics. Over the years, his research has been sponsored by various U.S. Federal agencies, including the U.S. Navy, the Air Force, the National Science Foundation, the Defense Health Agency, and the National Institute of Health.

Dr. Behdad was named the Harvey D. Spangler Faculty Scholar by the College of Engineering, from 2016 to 2019, and the H. I. Romnes Faculty Fellow by the Office of Vice Chancellor for Research and Graduate Education (OVCRGE), University of Wisconsin, from 2016 to 2021. He received five different fellowships and awards from the Office of Naval Research, the International Union of Radio Science (URSI), and the University of Michigan, Ann Arbor, among others. He was a recipient of the Vilas Associates Award from the OVCRGE of UW-Madison, in 2016, the 2014 R. W. P. King Prize Paper Award, the 2012 Piergiorgio L. E. Uslenghi Letters Prize Paper Award of the IEEE Antennas and Propagation Society, the CAREER Award from the U.S. National Science Foundation, in 2011, the Young Investigator Award from the U.S. Air Force Office of Scientific Research, and the Young Investigator Award from the U.S. Office of Naval Research. His graduate students were the recipients of 18 different awards/recognitions at various international symposia, including the IEEE AP-S/URSI Symposium, the USNC/URSI National Radio Science Meeting, the IEEE Pulsed Power and Plasma Science Symposium, and the Antenna Applications Symposium. He served as the Co-Chair of the Technical Program Committee of the 2012 the IEEE International Symposium on Antennas and Propagation and the USNC/URSI National Radio Science Meeting. He served as the General Co-Chair of the Fourth Arab-American Frontiers in Science, Engineering, and Medicine Symposium, in 2016. He also served as an Associate Editor for the IEEE Antennas and Wireless Propagation Letters, from 2011 to 2015.